Journal of Alloys and Compounds, *188* (1992) 87–93
JALCOM 9014

Preparation and characterization of melt-spun nickel-based alloys containing heavy metals

Soltane Lebaili
Institut de Génie Mécanique, USTHB, BP 32, El Alia, Bab-Ezzouar, Algiers (Algeria)

John Ajao
Centre for Energy Research and Development, Obafemi Awolowo University, Ile-Ife (Nigeria)

Sylvaine Hamar-Thibault
Institut National Polytechnique de Grenoble, Ecole Nationale Supérieure d'Electrochimie et d'Electrométallurgie de Grenoble, Laboratoire de Thermodynamique et Physico-chimie Métallurgiques (Unité de Recherche associée au CNRS 29), B.P. 75, 38402 Saint Martin d'Hères Cedex (France)

Abstract

The solidification behaviour and morphology of some nickel-based hardfacing alloys containing heavy metals such as tungsten have been studied by scanning electron microscopy and transmission electron microscopy. These alloys are very sensitive to different cooling rates (from as cast to melt spinning). At low cooling rates, these alloys present as primary phases, *i.e.* the stable carbide M_7C_3 or the double carbide M_6C (η type), according to the silicon content. For high cooling rates, the alloys occur as either amorphous (high silicon content) or microcrystallized structures depending on silicon level. In this latter case, the solid solution Ni(α) and the metastable carbide $M_{23}C_6$ are observed.

1. Introduction

The problem of wear and corrosion has been solved by hardfacing and other treatment of metals and steels. Hardfacing alloys containing several kinds of hard phase (carbides essentially, and borides or silicides) are used in several industries. To these new nickel-based alloys are added other non-metallic elements such as boron and silicon in order to improve the viscosity at high temperatures and to increase the hardness of the alloys. These hard phases are made up of chromium, tungsten and non-metallic elements (boron, silicon and carbon) [1, 2]. Of these nickel-, cobalt- or iron-based alloys, nickel-based hardfacing alloys are extensively patronized as a result of their autofluxing properties at high temperatures.

A good corrosion resistance of these alloys is assumed because of the presence of chromium while the wear resistance property is directly connected to the relations between the matrix and the hard phases: the nature (carbide, boride or silicide), the distribution, the form, the dimensions and the orientation relationship between the phases [3, 4]. The complexity of the beginning of solidification of these alloys makes them particularly sensitive to different solidification conditions [5].

Thus, in this present work, we are interested in the solidification behaviour and the stability of different phases of these alloys prepared by melt spinning. The nature of the composition of the different phases formed in these alloys will be observed using as-cast samples. These will serve as reference alloys in the discussion of the evolution of the microstructure after rapid solidification by melt spinning.

2. Experimental procedure

2.1. Preparation of the alloys

The solidification behaviour of different complex alloys was investigated. The compositions are given in Table 1. The alloys have been prepared in an electric furnace under a controlled atmosphere. The compositions of these alloys have been chosen with a large range of boron, silicon and carbon contents. The chromium content is maintained at around 25 at.% while that of tungsten is around 4 at.%.

These alloys are solidified by the technique of melt spinning which consists of induction melting the alloys in a crucible with a nozzle (diameter, 0.8 mm) through which the molten alloy is ejected on a rotating copper wheel under a helium pressure of about 200 mbar. The temperature of the liquid alloy before the ejection is kept at about 1350 °C. The wheel velocity varied from 15 to 28 m s^{-1}. The ribbons are 1–2 mm in width and

0925-8388/92/$5.00

TABLE 1. Composition of the alloys

Family	Amount (at.%) of the following elements					
	C	SI	B	CR	W	Ni
A	4.8	1.8	5.9	26.9	3.5	Balance
B	4.7	5.9	5.0	26.5	3.5	Balance

30–50 μm thick. The value of the heat transfer coefficient between the melt and the copper substrate is estimated at 10^5 W K^{-1} m^{-2} [6]. This low value corresponds to newtonian thermal transfer. The cooling rate can be estimated to be between 2×10^6 and 5×10^6 K s^{-1}. The annealing treatments of melt-spun ribbons have been carried out using a vacuum electric furnace.

2.2. Characterization of the alloys

The structure of the samples was examined by scanning electron microscopy (SEM) (JSM35 scanning electron microscope) equipped with an energy-dispersive X-ray analysis (EDXA) system (Tracor).

The nature of the phases as well as the microstructure were examined by X-ray and electron diffraction and by transmission electron microscopy (TEM) (JEM200CX transmission electron microscope) performed on thin foils. The thin foils were thinned electrolytically in an electrolyte containing a 9:1 acetic acid–perchloric acid solution at room temperature under 15 V and examined in a direction vertical to the ribbon surface. In addition to the general observations and electron diffraction performed on thin foils in TEM, EDXA and electron energy loss spectroscopy (EELS) at a resolution of 1.5 nm at the sample level were carried out. The EELS spectra (pulse-counting mode) were recorded using a Tracor-TN2000 multichannel system which is programmed for light element analysis such as boron and carbon.

3. Results and discussion

The alloys presented in Table 1 have compositions relatively similar to one another (except for the silicon content) but, given the number of metallic (nickel, chromium and tungsten) and non-metallic (carbon, boron and silicon) elements, the as-cast alloys can be grouped into two large families as a function of the primary phase formed during slow cooling.

3.1. Morphology of the slowly cooled samples

Following the relative carbon, boron and silicon contents, two primary phases have been observed in these alloys leading to the classification of the alloys into two families: alloys A with M_7C_3 as the primary phase; alloys B with the complex carbide M_6C as the primary phase.

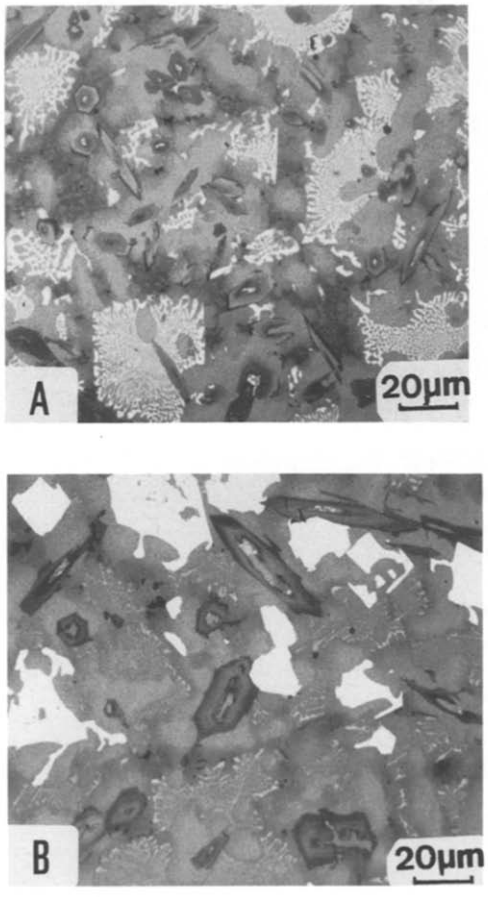

Fig. 1. General morphology of as-cast alloys A and B.

Alloys A have M_7C_3 as the primary phase during solidification (Fig. 1(a)). This carbide which is formed at an elevated temperature seems to depend little on the presence of the heavy elements. Its composition was almost constant $(Cr_{61}W_{2.5}Ni_{6.5})(B_2C_{28})$. No silicon was analysed and only 2 at.% B and 2–3 at.% W were soluble in this carbide. The tungsten level in this carbide was the same as in the alloy.

Alloys B are characterized by the formation, as primary phase, of a complex compound consisting of all the elements (except boron) in equivalent quantities. This phase appears in the micrograph in Fig. 1(b) as a large whitish phase in contrast with M_7C_3 which possesses a darkish colour. Its average formula $(Cr_{26}W_6Ni_{26}Si_{13})C_{14}$ $((CrW)_{2.3}(NiSi)_{2.8}C)$ approaches the double carbides of M_6C (η) type mentioned in the ternary Ni–W–C system [7]. In the Ni–W–C system, the η carbides had a nickel content range between 23 and 35 at.% at a constant carbon content of 14.3 at.%. Microprobe analyses performed on the η carbides formed in our samples show that the extents of their

nickel and carbon content ranges were similar: around 30 at.% Ni and between 13.5 and 16 at.% C.

The extension of the M_6C domain depends on carbon activity as reported for the quaternary Ni–Cr–W–C system [8] but no data were reported on the influence of silicon. It seems that silicon increases the extent of the composition range of these carbides as reported for cobalt-based alloys containing heavy metal where the η carbides were well known. Their compositions were very similar with around 33 at.% Ni + Co and between 6 and 13 at.% Si depending on the silicon level in the alloy [9].

The solidification process continues with the formation of different eutectics depending essentially on the nature of the primary phase and on the silicon level. In alloys A, the eutectics which form after the M_7C_3 consist of the same carbide rich in chromium and different chromium borides. As no silicon was soluble in M_7C_3, the silicon level was higher in the matrix than in the nominal composition (up to 4 at.%) and the solidification comes to an end by the formation of a fine binary eutectic between Ni(α) and Ni_3B.

In alloys B, the η carbide is surrounded by various binary eutectics formed at a high temperature: Ni(α)–M_7C_3 and Ni(α)–Cr_xB ($1.5 < x < 2.0$). Even though this phase has a high silicon content, the silicon content in the solid solution of nickel can reach 10 at.%. This important segregation then allows the crystallization of the ternary eutectic between the three phases Ni(α), Ni_3B and Ni_5Si_2 at the end of solidification, as expected from the ternary Ni–Si–B system [10].

3.2. *Macrostructure of the melt-spun alloys*

In general, melt-spun ribbons present a microstructure showing the existence of three principal zones [11–15].

(1) A quenched zone in contact with the wheel is microcrystallized and shown to occur in these alloys. This zone towards the wheel side corresponds to the stage when the cooling rate is extremely high. The interface temperature is very much lower than the temperature of the melt.

(2) A columnar zone extends over the rest of the thickness of the ribbons. The columnar dendrites are in general parallel to themselves. During solidification, the latent heat release of crystallization causes an increase in the interface temperature, the undercooling is reduced and the solidification rate is much decreased. This stage of solidification gives rise to the formation of the second zone with the development of well-oriented dendrites with respect to the thermal gradient.

(3) A dendritic equiaxed zone develops from the free wheel side of the ribbon. The observation of this rather thin zone depends also on different factors. The observations of the two zones (quench and equiaxed) depends essentially both on the nature of the alloy and on the cooling rate [12–15].

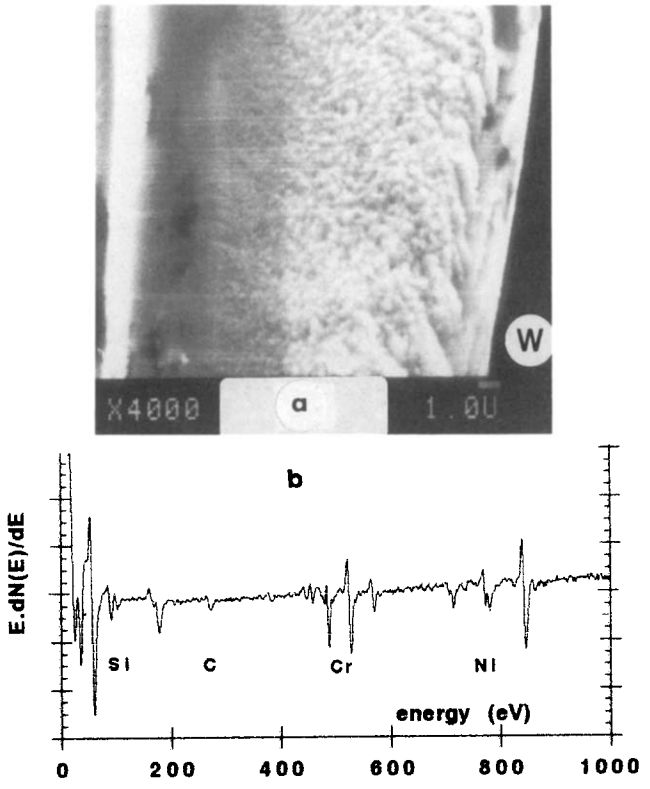

Fig. 2. (a) Microstructure of section of the ribbons of melt-spun alloy A ($V_r = 28\ m\ s^{-1}$): W, wheel side. (b) Auger spectrum between 15 and 1000 eV obtained on the wheel side of alloy A.

Many researchers [16, 17] working on nickel-based alloys have observed only two zones: quenched and columnar dendritic zones. In agreement with the results of these workers, alloys A and B present only these two zones as shown in Fig. 2(a). The first zone towards the wheel side (of thickness between 5 and 15 μm) shows no particular structure while, towards the free wheel side, a microcrystallized zone can be observed. In all the other alloys, the first zone towards the free wheel side is microcrystallized followed by a dendritic equiaxed zone towards the free wheel side of the ribbon. These observations were confirmed by X-ray diffraction experiments. In alloys B, the diffractogram obtained on the wheel side of the ribbon shows a completely amorphous structure while that obtained on the free wheel side shows some peaks identifiable as nickel. In alloys A, the diffractogram obtained on the free wheel side or on the wheel side of the ribbon show the presence of some peaks which can be indexed as nickel.

The rolling velocity V affects the thickness e of the ribbon. An attempt was made to correlate these two values. Hillman and Hilzinger [18] proposed a relation of the following type: $e = V^{-p}$ where p depends on the nature of the thermal transfer during cooling. p is equal to 0.75 for perfect cooling and to 1.5 for newtonian cooling. We found experimentally that $p = 1.0$ which

corresponds to an intermediate thermal transfer. The morphology of the alloys confirms the low coefficient of heat transfer for the apparatus and the existence of the intermediate mode of heat transfer between the substrate and the melt.

The Auger spectra obtained on the two sides of the ribbons of alloys A and B are very similar. Silicon, chromium and nickel peaks are well resolved even before sputtering, as shown in Fig. 2(b). After the removal of the contamination layer, the spectrum show the bulk composition of the alloys. Weak segregation was found at the ribbon level. The tungsten and chromium concentrations were slightly lower at the wheel side surface of the ribbon irrespective of the type of the alloy. A similar observation was found concerning the silicon concentration; the peak is higher at the wheel side than at the free wheel side of the ribbon. It is difficult to correlate this segregation with the different zones observed across the ribbons.

3.3. *Microstructure of the melt-spun alloys A*

The fine microstructure of alloy A obtained by TEM and analysed by scanning transmission electron microscopy (STEM)–EDXA shows the presence of three phases. The STEM micrograph (Fig. 3(a)) shows the microcrystallized structure in the form of a daisy towards the free wheel side of the ribbon. The size of the daisy is about 600 nm. EDXAs carried out on thin foils show the presence of at least three types of grain having very different compositions (Fig. 3(c)).

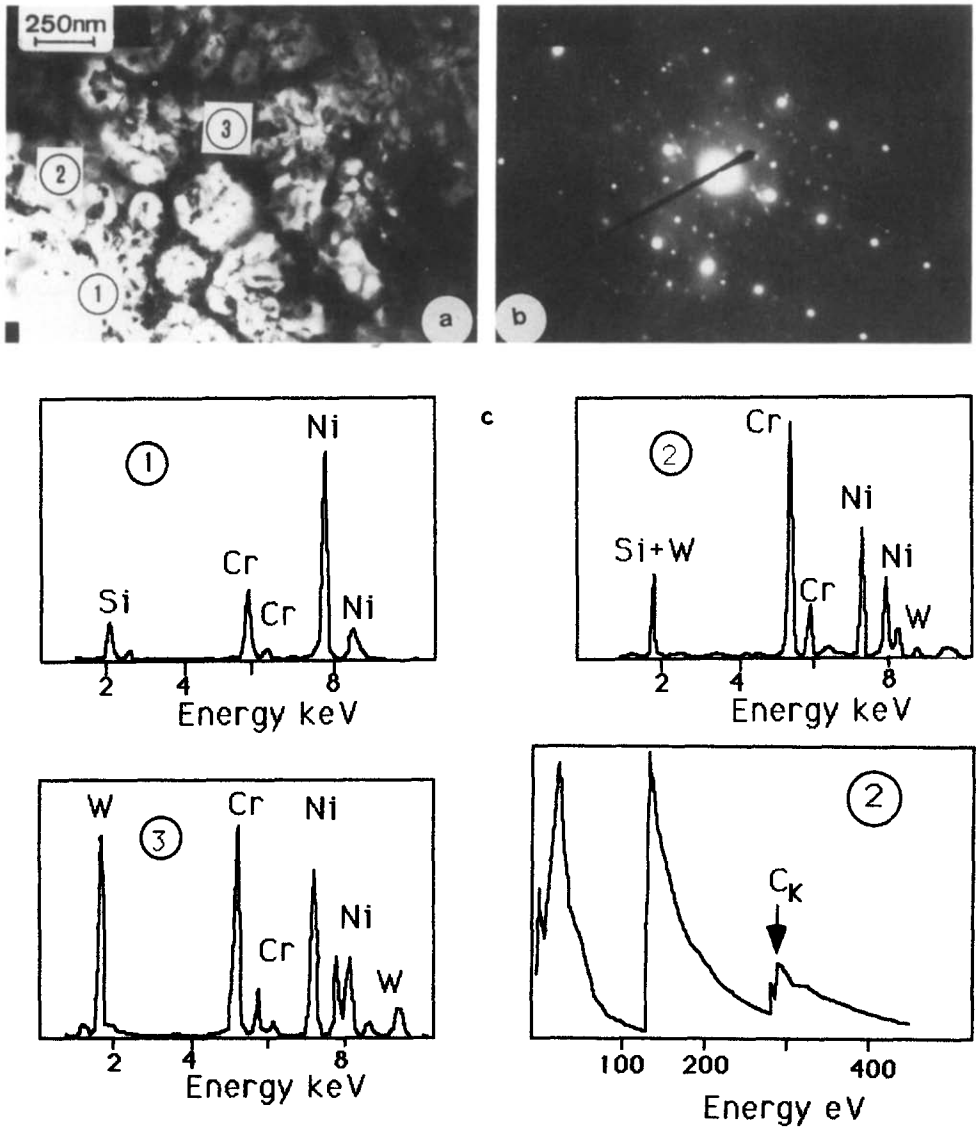

Fig. 3. TEM observations on the free wheel side of the ribbon of alloy A: (a) microstructure; (b) electron diffraction pattern; (c) microanalyses consisting of EDXA on area 1, 2 and 3 and EELS analyses on area 2.

(1) In the heart of the daisy, the presence of the major phase corresponding to the solid solution Ni(α) (f.c.c.) is analysed (area 1).

(2) As one moves towards the external part of this zone, we observed the presence of a chromium-rich phase as shown in the EDXA spectrum 2. The EELS spectrum obtained in this zone show that the only light element detected is carbon. The presence of the metastable $M_{23}C_6$ (a = 10.6 Å) is confirmed by the electron diffraction patterns obtained by electron diffraction (Fig. 3(b)). This carbide replace in melt-spun alloys the M_7C_3 observed in slowly cooled alloys. The good match between the f.c.c. structure of nickel and the f.c.c. structure of the $M_{23}C_6$ (the lattice parameter of nickel is almost one third that of $M_{23}C_6$) could promote the nucleation of the cubic carbide whereas the hexagonal M_7C_3 was thermodynamically the stable phase. The formation of cubic metastable phases has been observed in different ternary systems such as Fe–Ni–B [19] or Ni–B–Si [20].

(3) An interdendritic space was detected. This inter-daisy space is a phase which appears whitish in the bright field image and extremely rich in tungsten as shown in the EDXAs (area 3). This phase could probably be identified as the M_6C. The low carbon levels do not allow unambiguous detection by EELS.

As shown in previous work [21], the carbon signal observed in Auger spectroscopy decreased but residual carbon was detected. The fine structure of the carbon peak appearing at a low energy indicates that carbon was bound in agreement with the TEM observation of $M_{23}C_6$.

3.4. *Microstructure of the melt-spun alloys B*

Alloys B melt spun with a wheel velocity of about 32 m s^{-1} show essentially an amorphous matrix inside which are some isolated crystallites of about 500 nm (Fig. 4(a)).

The electron diffraction pattern in this region confirmed effectively an amorphous structure with some microcrystallized zones (Fig. 4(b)). It should be noted that the wheel side of the ribbon is poorer in crystallites. Further observations of these crystallites by STEM–EDXA show that they are made up of small crystals about 10 nm in size. The EDXAs performed on these crystallites allow the identification of nickel, chromium and tungsten (Fig. 4(c)). The chromium-to-nickel ratio obtained by EDXAs of around 0.50 is in good agreement with the global composition of the alloy (chromium-to-nickel ratio, 0.47). In the EELS analyses performed on the ribbon, the only light element detected is carbon in the amorphous region (Fig. 4(c)) whereas,

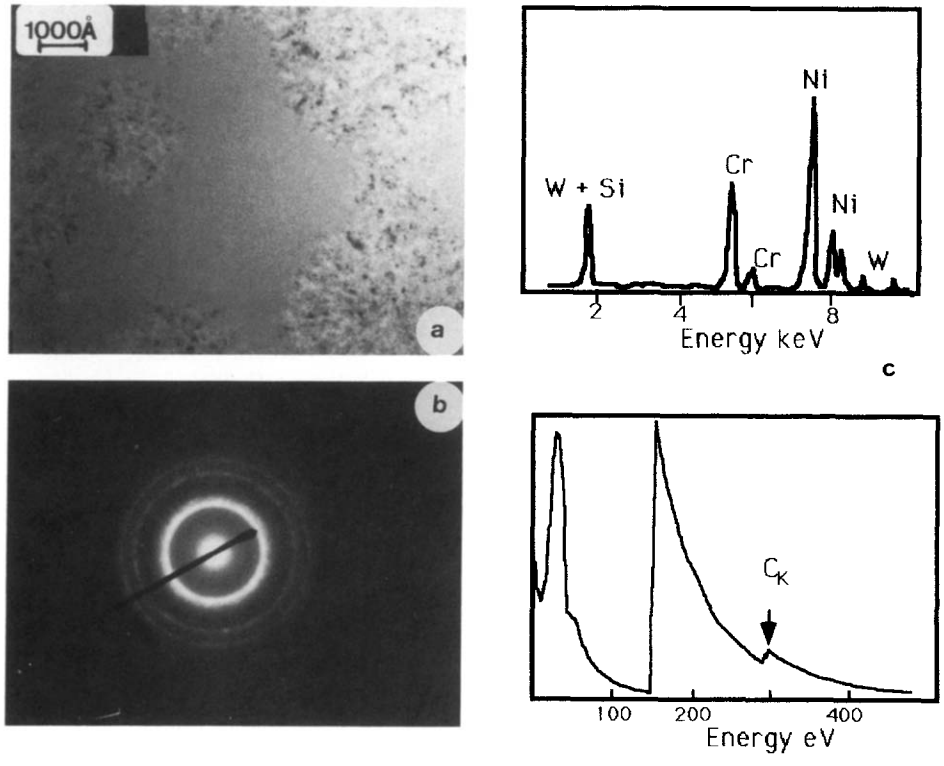

Fig. 4. (a) Microstructure of melt-spun alloy B showing some crystallites in the amorphous matrix; (b) electron diffraction pattern; (c) EDXA–STEM and EELS microanalyses.

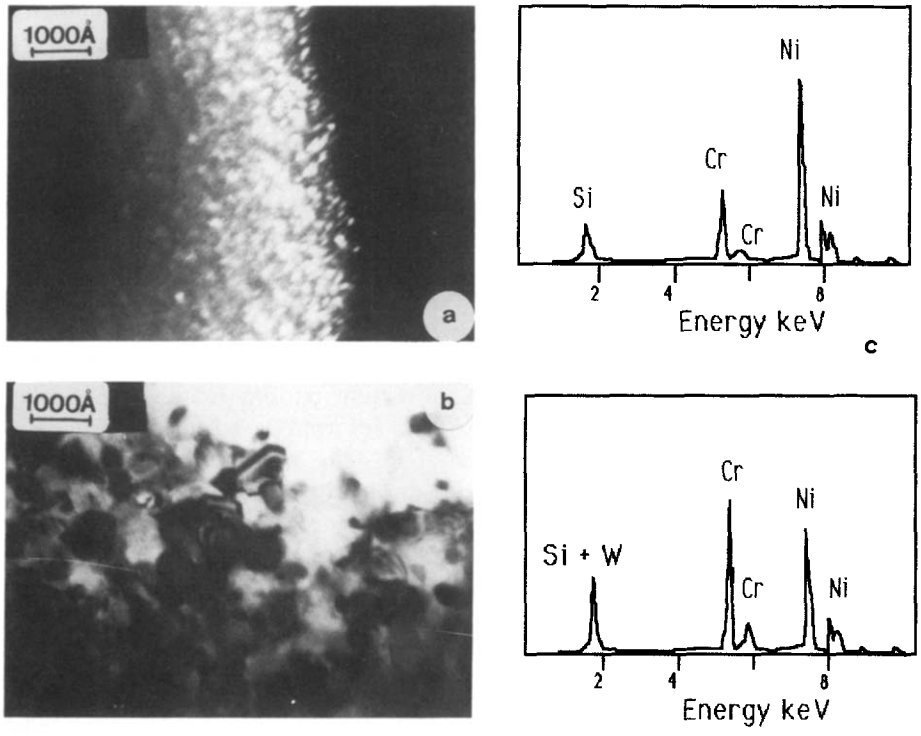

Fig. 5. Structure and STEM–EDXA microanalyses obtained for melt-spun alloy B heat treated at (a), (b) 480 K for 24 h and (c) at 625 K.

in the crystallite region, no light element was in evidence, which probably implies the presence of crystallites dominated by a nickel solid solution.

This alloy which has been annealed at 625 K for 24 h produced a large crystal size (100 nm). According to the STEM–EDXA performed on these heat-treated samples (Fig. 5), we are able to identify two types of grain.

(1) A darkish grain in the bright field image which is particularly rich in nickel and chromium is identified as the solid solution of Ni(α).

(2) Another whitish phase in the bright field image which is particularly rich in tungsten, silicon, chromium and nickel has an average composition which approaches that of the η carbide obtained in the same alloy under slow cooling. The grain size increases with increasing annealing temperature.

Alloy B melt spun with a lower velocity ($15\ m\ s^{-1}$) shows a completely microcrystallized structure similar to the structure of alloy A.

From our observations, the silicon content seems to be an important factor for amorphization; a high silicon content promotes glass formation in these complex alloys. These results agree with observations made on the ternary Ni–B–Si system where silicon additions increase the composition range where glasses can be formed [22]. Moreover the observation of an amorphous zone on the wheel side can be correlated with both the high cooling rate and the higher silicon level reported above.

4. Conclusion

In the present work, the influence of silicon on the structure of complex alloys containing heavy metal has been shown. In slowly cooled alloys, the nature of the primary phase (M_7C_3 or M_6C) is directly related to the silicon content. Depending on the cooling rate and on the composition, melt-spun alloys are either amorphous or microcrystallized with the formation in microcrystallized alloys of metastable phases such as $M_{23}C_6$.

References

1 *Metals Handbook*, Vol. 6, *Welding and Brazing*, American Society for Metals, Metals Park, OH, 1966.
2 E. A. Antonova, N. S. Andruhschenko and L. M. Sinai, *Zashch. Met.*, *8* (1972) 538.
3 O. Knotek, E. Lugscheider and H. Reiman, *J. Vac. Sci. Technol.*, *12* (1975) 770.
4 O. Knotek, E. Lugscheider and W. Wichert, *Thin Solid Films*, *53* (1978) 303.
5 S. Lebaili and S. Hamar-Thibault, *Mém. Sci. Rev. Metall.*, *81* (1984) 519.
6 P. Casanona, J. C. Joud and C. Senillou, *Mém Sci. Rev. Métall.*, *81* (1984) 553.
7 M. L. Fiedler and H. H. Stadelmaier, *Z. Mettallkd.*, *66* (1975) 402.
8 K. Masanori, *J. Iron Steel Inst. Jpn.*, *68* (1982) 1355.
9 M. Durand-Charre, S. Hamar-Thibault and B. Andries, *Mém. Sci. Rev. Metall.*, *78* (1981) 321.
10 S. Lebaili and S. Hamar-Thibault, *Acta Metall.*, *30* (1987) 501.

11 T. W. Clyne, in P. Sahm, (ed.), *Proc. Workshop on Nucleation and Rapid Solidification, Aachen, 1983*, Hungary 1983 p. 96.
12 M. Blank, C. Caersar and U. Köster, in S. Steeb and H. Warlimont (eds.), *Proc. 5th Int. Conf. on Rapidly Quenched Metals*, North-Holland, Amsterdam, 1985, p. 883.
13 A. Remy and F. Frantz, *Mém. Sci. Rev. Métall.*, (1987) 265.
14 F. Fayard, F. Duflos and A. Lasalmonie, in S. Steeb and H. Warlimont, (eds), *Proc. 5th Inst. Conf. on Rapidly Quenched Metals*, North-Holland, Amsterdam, 1985, p. 811.
15 J. Ajao, J. Desseaux and S. Hamar-Thibault, *J. Mater., Sci., 24* (1989) 3647.
16 H. A. Davis, N. Shohoji and D. H. Warrington, *Proc. 2nd Int. Conf. on Rapid Solidification Processing: Principles and Technologies, Reston*, VA, *1980*, Clark's Publishing Division, Baton Rouge, LA, 1980, p. 153.
17 F. Duflos and J. F. Stohr, *J. Mater. Sci., 7* (1982) 3641.
18 M. Hillman and H. R. Hilzinger, in B. Cantor (ed.), *Proc. 3rd Int. Conf. on Rapidly Quenched Metals*, Vol. 1, Metals Society, London, 1978, p. 22.
19 U. Koster, in B. H. Kear, B. C. Giessen and M. Cohen (eds.), *Rapidly Solidified Amorphous and Crystalline Alloys*, North-Holland, Amsterdam, 1982, p. 179.
20 D. G. Morris, *J. Mater. Sci., 20* (1985) 331.
21 S. Hamar-Thibault, J. Ajao and S. Lebaili, *Proc. 4th Eur. Conf. on Applications of Surface and Interface Analysis, Budapest, 1991*, Hungary 1991, p. 391.
22 I. W. Donald and H. A. Davis, *J. Mater. Sci., 15* (1980) 2754.